Double Echo Symmetry-Based REDOR and RESPDOR Pulse Sequences for Proton Detected Measurements of Heteronuclear Dipolar Coupling Constants

Benjamin A. Atterberry [1,2], Scott L. Carnahan [1,2], Yunhua Chen,[1,2] Amrit Venkatesh [1,2] and Aaron J. Rossini [1,2]*

[1]*US DOE Ames Laboratory, Ames, Iowa, USA, 50011*
[2]*Iowa State University, Department of Chemistry, Ames, IA, USA, 50011*

Corresponding Author:
*Email: arossini@iastate.edu

Abstract

^{1}H{X} symmetry-based rotational echo double resonance pulse sequences (S-REDOR) and symmetry-based rotational echo saturation pulse double resonance (S-RESPDOR) solid-state NMR experiments have found widespread application for ^{1}H detected measurements of difference NMR spectra, dipolar coupling constants, and internuclear distances under conditions of fast magic angle spinning (MAS). In these experiments the supercycled $R4_1^2$ ($SR4_1^2$) symmetry-based recoupling pulse sequence is typically applied to the ^{1}H spins to reintroduce heteronuclear dipolar couplings. However, the timing of $SR4_1^2$, and other symmetry-based pulse sequences must be precisely synchronized with the rotation of the sample, otherwise, the evolution of ^{1}H CSA and other interactions will not be properly refocused. For this reason, significant distortions are often observed in experimental dipolar dephasing difference curves obtained with S-REDOR or S-RESPDOR pulse sequences. Here we introduce a family of double echo (DE) S-REDOR/S-RESPDOR pulse sequences that function in an analogous manner to the recently introduced t_1-noise eliminated (TONE) family of dipolar heteronuclear multiple quantum coherence (D-HMQC) pulse sequences. Through numerical simulations and experiments the DE S-REDOR/S-RESPDOR sequences are shown to provide dephasing difference curves similar to those obtained with S-REDOR/S-RESPDOR. However, the DE sequences are more robust to the deviations of the MAS frequency from the ideal value that occurs during typical solid-state NMR experiments. The DE sequences are shown to provide more reliable ^{1}H detected dipolar dephasing difference curves for nuclei such as ^{15}N (with isotopic labelling), ^{183}W and ^{35}Cl. The double echo sequences are therefore recommended to be used in place of conventional REDOR/RESPDOR sequences for measurement of weak dipolar coupling constants and long-range distances.

Introduction

High-resolution magic angle spinning (MAS) solid-state nuclear magnetic resonance (SSNMR) is a powerful technique for probing molecular structure and dynamics in organic solids, inorganic materials, and biomolecules.[1-3] The ability to routinely measure homonuclear and heteronuclear dipolar coupling constants is one of the most powerful features of SSNMR spectroscopy. The dipolar coupling constant (d_{ij}) for two coupled spins *i* and *j* is given by:

$$d_{ij} = -\frac{\mu_0 \hbar \gamma_i \gamma_j}{8\pi^2 r_{ij}^3} \qquad (1)$$

where γ is the gyromagnetic ratio of each spin, r_{ij} is the internuclear distance of the coupled spins, and d_{ij} has units of Hz. Hence, measurement of dipolar coupling constants in rigid systems allows the determination of internuclear distances, which are invaluable for molecular structure determination.[4-15] In favorable cases, measurement of dipolar coupling constants enables the location of atoms with precision rivaling that of diffraction techniques.[16] In systems with known structures/internuclear distances, the knowledge of dipolar coupling constants can be used to assess dynamics.[17-22]

A large number of methods exist for the high-resolution solid-state NMR measurements of homonuclear and heteronuclear dipolar coupling constants.[23-35] Only a fraction of the existing methods are cited here because of space constraints. There are several detailed review articles on dipolar recoupling and other pulse sequences for dipolar coupling constant measurements.[36-40] Dipolar coupling constants have traditionally been measured with solid-state NMR experiments performed with rotors capable of magic angle spinning at frequencies below 20 kHz.[23-35] Consequently, moderate or low-γ nuclei such as ^{13}C, ^{15}N, ^{31}P, etc. were detected since they give rise to well-resolved solid-state NMR spectra, permitting site-specific measurements of dipolar coupling constants.

In the past 20 years, the development of reduced diameter rotors capable of fast MAS frequencies above 30 kHz has permitted the more routine use of ^{1}H detected solid-state NMR experiments.[41-44] ^{1}H detected fast MAS NMR experiments provide two clear advantages: First, MAS at frequencies comparable to or exceeding the magnitude of homonuclear ^{1}H dipolar coupling constants results in extended ^{1}H coherence lifetimes and enhanced spectral resolution.[41-44] Second, detection of ^{1}H spins can provide order of magnitude gains in sensitivity as compared to NMR experiments employing detection of lower-γ spins.[41,43,45,46] For these reasons, ^{1}H detection has also been extended to high-*Z* spin-1/2 nuclei which possess very large chemical shift anisotropies (e.g., ^{119}Sn, ^{195}Pt, ^{199}Hg, ^{207}Pb, etc.),[47-52] and low-γ spin-1/2 nuclei.[41,43,46,53,54] Indirect detection (including of ^{1}H spins) allows NMR experiments with integer and half-integer quadrupolar nuclei which are challenging or impossible to directly detect.[14,33,55-67]

One of the most popular pulse sequences for ^{1}H detected measurement of heteronuclear dipolar coupling constants is the symmetry-based rotational echo double resonance pulse sequences (S-REDOR, Figure 1A).[31,34] The S-REDOR experiment consists of a ^{1}H spin echo with recoupling applied symmetrically about the central π-pulse. Application of an inversion pulse to a dipole-coupled heteronucleus results in the maximum reduction of the ^{1}H NMR signal. When S-REDOR is applied to measure dipolar couplings to quadrupolar spins in which all transitions cannot be inverted, but rather, can only be (partially) saturated, it is denoted as the symmetry-based rotational echo saturation pulse double resonance (S-RESPDOR).[58,68] In the S-RESPDOR experiment the π-pulse on the dephased nucleus is replaced with a saturation pulse which is often 1.5 or more rotor cycles in duration.[58,64,68,69] Currently, the most commonly applied dipolar recoupling sequence for fast MAS S-REDOR and D-HMQC experiments is the

supercycled $R4_1^2$ pulse sequence ($SR4_1^2$).[29] $SR4_1^2$ offers good robustness to ^1H RF inhomogeneity and has a scaling factor of 0.27, and typically provides better efficiency/higher dephasing than alternative recoupling sequences such as rotary resonance recoupling (R^3).[70] By recording a series of $^1H\{X\}$ S-REDOR/S-RESPDOR spectra with increasing recoupling durations and monitoring the dephasing of the ^1H signal it is possible to construct a dipolar dephasing curve. The dephasing curve can then be fit using numerical simulations or analytical functions to extract dipolar coupling constants.

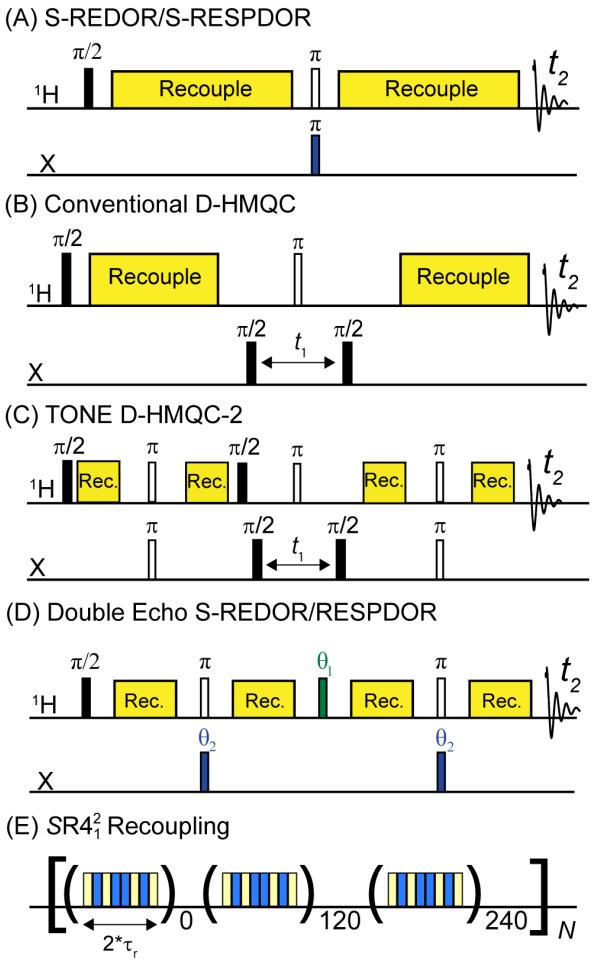

Figure 1. $^1H\{X\}$ S-REDOR/RESPDOR and D-HMQC pulse sequences. (A) S-REDOR/S-RESPDOR, (B) conventional D-HMQC, (C) TONE D-HMQC-2 (D) double echo (DE) S-REDOR/S-RESPDOR. In this work, $SR4_1^2$ recoupling was applied in all cases. (E) $SR4_1^2$ recoupling consists of 180° phase-alternated π-pulses. Each $R4_1^2$ block has a total duration of two rotor cycles consisting of eight π-pulses, each of which has a duration of $0.25 \times \tau_r$. A 120° phase shift is applied to each $R4_1^2$ block, with 3-blocks total required to complete the supercycle.

Unfortunately, recoupling pulse sequences for heteronuclear dipolar coupling also recouple chemical shift anisotropy (CSA) because these two interactions have the same symmetry.[32] In an S-REDOR experiment the evolution of ^{1}H CSA is refocused by the central π-pulse applied on the ^{1}H spin (Figure 1A). However, in order for the ^{1}H CSA to correctly refocus, the timing of the pulse sequence must be precisely synchronized with the magic angle spinning. As we have recently shown for ^{1}H{X} D-HMQC experiments with $SR4_1^2$ recoupling (Figure 1B), random fluctuations of the MAS frequency of even a few Hz can cause large variations in the intensity of the NMR signal from scan to scan.[66] This observation explains why conventional ^{1}H detected D-HMQC (and by extension S-REDOR) pulse sequences where $SR4_1^2$ recoupling is applied on the observed ^{1}H spin give rise to significant t_1-noise and/or random fluctuations of signal intensities, preventing the reliable measurement of 2D NMR spectra/dipolar dephasing curves. We recently introduced the t_1-noise eliminated (TONE) family of D-HMQC pulse sequences which provide 2D NMR spectra with better sensitivity than conventional D-HMQC.[49,66] In the TONE D-HMQC pulse sequence, a ^{1}H π-pulse is applied in the middle of each ^{1}H dipolar recoupling block to refocus ^{1}H CSA evolution (Figure 1C), making the sequence more tolerant to asynchronous sample rotation, and allowing the use of purge or trim pulses to eliminate uncorrelated ^{1}H magnetization. Alternatively, in experiments such as TRAPDOR[55,71,72] and T-HMQC,[73,74] recoupling is performed by applying high-power saturation pulses to the indirectly detected quadrupolar spins. These TRAPDOR-based sequences appear to be more robust to MAS frequency fluctuations and give less t_1-noise than sequences where recoupling is applied to the observed spin.[74] However, applying the recoupling to the indirect channel is not a general approach because the RF field and offset of the recoupling pulse needs to be optimized for different samples and nuclei. Additionally, applying recoupling to the

indirectly detected spin may lead to slower and/or lesser dephasing because the saturation of the quadrupolar spin will strongly depend upon the quadrupolar interaction parameters of the irradiated spin. Schmedt auf der Günne and co-workers demonstrated a REDOR sequence where *C*-type symmetry based recoupling was applied on the dephased spin was tolerant of MAS frequency deviations.[75] But, this sequence can only be applied when the dephased nucleus is spin-1/2.

Here we introduce a family of double echo (DE) S-REDOR pulse sequences, which have similar symmetry to the TONE D-HMQC pulse sequences (Figure 1D). We show through numerical simulations and experiments that these pulse sequences are much more tolerant towards MAS frequency variations. Furthermore, for dipolar coupled spin-1/2 nuclei, it is possible to control the rate and extent of dephasing by using different combinations of pulse tip angles on ^{1}H and indirectly detected spin. Overall, DE S-REDOR sequences with $\mathit{S}\mathrm{R}4_1^2$ recoupling are shown to provide robust ^{1}H detected dipolar dephasing measurements.

Results & Discussion

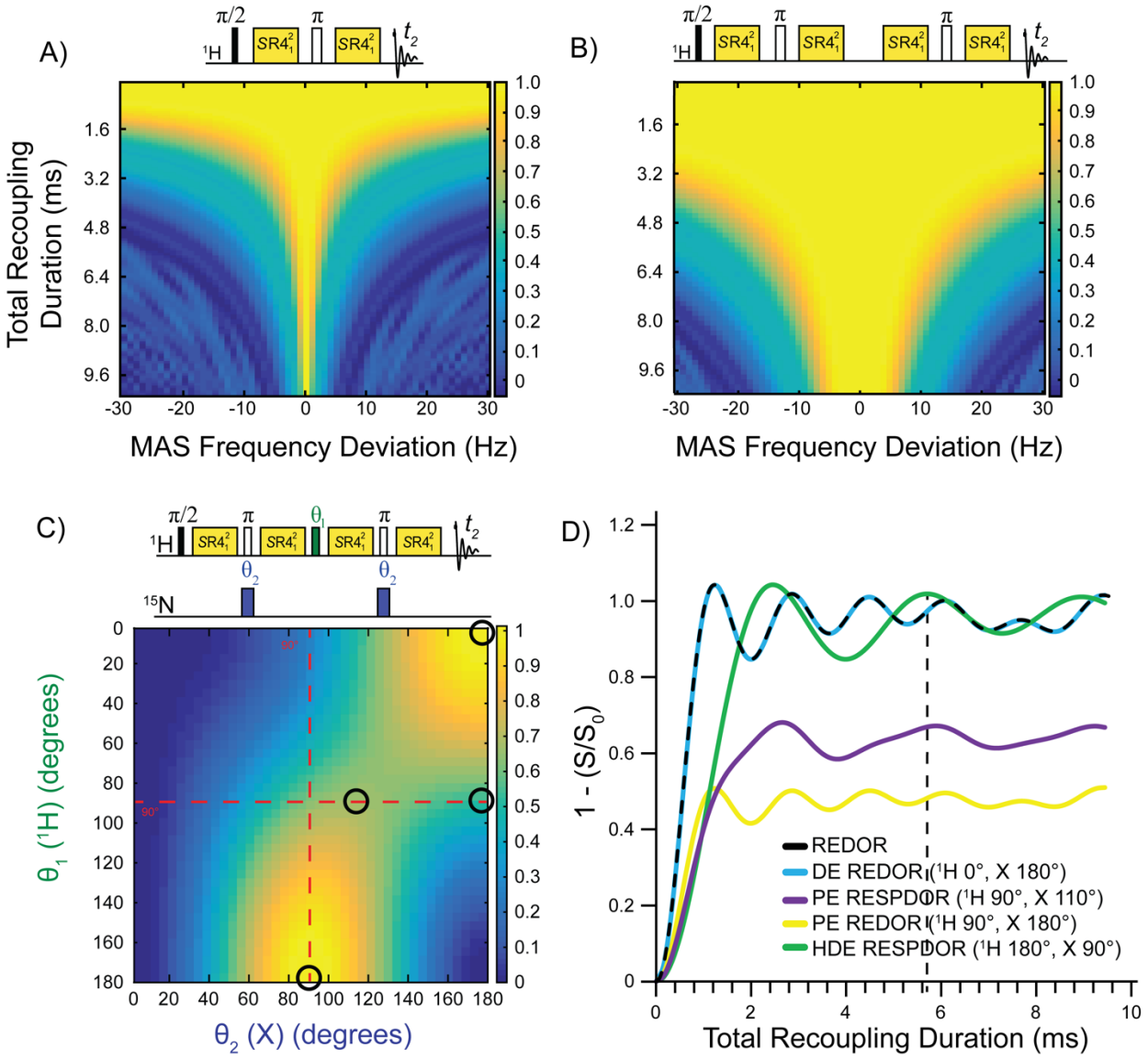

Figure 2. SIMPSON calculated ^{1}H NMR signal intensity as a function of the deviation of the MAS frequency from an ideal value of 50 kHz for (A) REDOR and (B) DE REDOR with $SR4^2_1$ dipolar recoupling. The ^{1}H reduced chemical shift anisotropy (δ_{CSA}) was 10 ppm (~4000 Hz). (C) SIMPSON simulated values of $\Delta S/S_0$ for different pulse tip angle combinations with a 50 kHz MAS frequency, 5.76 ms of $SR4^2_1$ dipolar recoupling and a ^{1}H-^{15}N dipolar coupling constant of 2500 Hz. (D) Simulated ^{1}H{^{15}N} dipolar dephasing difference ($\Delta S/S_0$) curves for REDOR, DE REDOR, PE REDOR, PE RESPDOR, and HDE RESPDOR.

Numerical Simulations of S-REDOR Pulse Sequences. Figure 2A and 2B show pulse sequence diagrams and numerically simulated heat plots for S-REDOR and DE S-REDOR, respectively, that display the control signal intensity (S_0) as a function of the total duration of

$SR4_1^2$ recoupling and the deviation of the MAS frequency from the ideal value of 50 kHz. From this point forward, S-REDOR/S-RESPDOR are simply denoted as REDOR/RESPDOR and DE S-REDOR/DE S-RESPDOR are denoted DE REDOR/DE RESPDOR. In these simulations, the pulse timings and durations are calculated based upon an MAS frequency of 50 kHz, while the input MAS frequency was varied from 49970 to 50030 Hz. The heat plots clearly illustrate that the double echo REDOR pulse sequence is more tolerant to deviations of the MAS frequency from the ideal value than the standard REDOR pulse sequence, especially at longer recoupling durations. Figure S1 shows additional simulations with different values of the ^{1}H CSA and ^{1}H-^{15}N dipolar coupling constants. As expected, larger values of the ^{1}H CSA make the REDOR and DE REDOR experiments more sensitive to MAS frequency fluctuations. Additionally, increased dipolar coupling constants also result in increased sensitivity to MAS frequency deviations. Regardless of the values of ^{1}H CSA or heteronuclear dipolar coupling constant, the DE REDOR pulse sequence always offers improved robustness (Figure S1).

When analyzing REDOR experiments the normalized dipolar dephasing difference curve ($\Delta S/S_0$) is usually calculated with the following equation:

$$Normalized\ Dephasing\ Difference = \Delta S/S_0 = 1 - \frac{S}{S_0} \qquad (1)$$

where S_0 is the control signal intensity (no pulses on the X nucleus), and S is the dephased signal intensity (inversion/saturation pulses applied on the X-channel nucleus). The analysis in Figure 2A and Figure 2B focus on the control signal intensity (S_0) because it is most sensitive to deviations of the MAS frequency. On the other hand, the dephased signal intensity (S) does not show large changes in magnitude with deviations of the MAS frequency (Figure S2). Hence, a reduction in S_0 brought about by MAS instability of even a few Hz would be expected to lead to a decrease in $\Delta S/S_0$. Indeed, as shown below in Figure 3, the experimental ^{1}H{^{15}N} REDOR and

DE REDOR $\Delta S/S_0$ curves decrease in intensity at longer recoupling durations. We note that there are several published examples of ^{1}H{X} $\Delta S/S_0$ REDOR curves which decay at longer recoupling times.[51,64] See below for further discussion of the experimental data.

Monte Carlo Analysis of Numerical Simulations. We previously used a Monte Carlo analysis of numerical SIMPSON simulation outputs to demonstrate how TONE D-HMQC provides improved robustness to MAS frequency deviations and reduces t_1-noise.[66] A similar Monte Carlo analysis was used to analyze the data in Figure 2 and Figure S2 and construct S, S_0, ΔS curves for REDOR and DE REDOR that mimic the imperfect MAS frequency stability present in experiments and illustrate why DE REDOR provides more stable $\Delta S/S_0$ curves. Briefly, a script was written in MATLAB to analyze the SIMPSON calculated control (S_0) and dephased (S) and dephasing difference ($\Delta S/S_0 = 1 - S/S_0$) signal intensities as a function of the recoupling time (the MATLAB script is provided as Supplementary Material). The user first inputs the standard deviation of the MAS frequency (σ_{MAS}, 6 Hz was used here). For a given recoupling duration, the script randomizes the MAS frequency based upon a Gaussian probability distribution, looks up the corresponding S and S_0 signal intensities and adds them to previously determined values of S and S_0 to mimic the signal averaging that occurs for each recoupling duration. The signal averaged values of S and S_0 are then used to calculate $\Delta S/S_0$ for each recoupling duration.

Figure S3 summarizes the Monte Carlo analysis of REDOR and DE REDOR numerical simulations. In all analyses 128 scans were used with a 6 Hz MAS frequency standard distribution. Both REDOR and DE REDOR show decreasing values of S_0 signals as the recoupling duration is increased, however, DE REDOR offers higher values of S_0 due to its improved stability. However, for both REDOR and DE REDOR the values of S are

also predicted to decrease in the presence of MAS instability. We note that at some longer recoupling durations, the value of S becomes slightly negative, consequently the analysis predicts that the dephasing difference will actually increase in the presence of MAS instability. However, in reality, $\Delta S/S_0$ values greater than one (S values below zero) are usually not observed, likely because both signal overlap and imperfections such as radiofrequency field inhomogeneity reduce $\Delta S/S_0$. Consequently, simulations were also performed where S values were scaled in the following way prior to the randomization of MAS frequencies and subsequent calculations:

$$S_{scaled} = f \times S + (1 - f) \qquad (2)$$

With scaling factors (f) of 0.9 or 0.95, S_{scaled} is generally above 0 at all recoupling durations. When using S_{scaled} the Monte Carlo analysis now correctly predicts that REDOR yields $\Delta S/S_0$ curves that decrease at longer recoupling durations because of the reduction in S_0. In disagreement with the experiment, the Monte Carlo analysis predicts that DE REDOR curves will never decay, regardless of the scaling factor. There are several experimental factors absent from our analysis which could explain this discrepancy. For example, effects such as homonuclear ^{1}H-^{1}H dipolar coupling, heteronuclear dipolar coupling to abundant spins such as ^{14}N, and RF inhomogeneity are not modeled. Additionally, we assume that the MAS frequency is constant for each scan; it is unclear what the effect of varying the MAS frequency would be over the duration of a recoupling block as this is challenging to incorporate into the numerical calculations.

In summary, the Monte Carlo analysis predicts that if the MAS frequency deviates from the ideal value by even a few Hz, the intensity of the S_0 signal will decrease at longer recoupling durations. The decrease in S_0 is significantly lessened with the DE REDOR pulse

sequence. Consequently, DE REDOR is more robust with respect to MAS frequency deviations, explaining why it yields $\Delta S/S_0$ curves that are more stable at long recoupling durations.

Variation of Pulse Tip Angles in DE REDOR Pulse Sequences. With the double echo family of REDOR pulse sequences it is also possible to employ pulses with different tip angles on the dephased spin and to vary the tip angle of the central refocusing pulse on the observed spin. Figure 2C is a heat plot that shows the numerically simulated dephasing for different tip angle combinations on the ^{1}H and X channel (^{15}N in this case). Note that on this plot, an intensity of 1.00 corresponds to maximum dephasing (S signal ≈ 0). For these simulations the dipolar coupling constant was 2500 Hz and the recoupling duration of 5.760 ms (indicated by the vertical dashed line on Figure 2D) was chosen so that dephasing was maximized for all tip angles. Maximum dephasing of 1.0 is observed with (^{1}H $\theta_1 = \pi$, X $\theta_2 = \pi/2$) and (^{1}H $\theta_1 = 0$, X $\theta_2 = \pi$), and ~70% dephasing is observed for (^{1}H $\theta_1 = \pi/2$, X $\theta_2 = 110°$); where θ_1 and θ_2 denotes the tip angle of the pulse applied on the ^{1}H channel and X channel, respectively. From this point, if $\theta_1 = 0$ (i.e., no central ^{1}H pulse is applied) the pulse sequence is denoted as DE REDOR or DE RESPDOR when inversion pulses or saturation pulses are applied on the X channel, respectively. If $\theta_1 = \pi/2$ the pulse sequence is denoted as a perfect echo (PE). The sequence is called PE REDOR or PE RESPDOR, for $\theta_2 = \pi$ and $\theta_2 = 110°$, respectively. The name PE RESPDOR is also used when a longer duration saturation pulse is used, as is the case for quadrupolar nuclei, see below. For the subsequent PE RESPDOR experiments and simulations with ^{15}N, θ_2 was set to 110° because this tip angle maximizes dephasing when $\theta_1 = \pi/2$. If $\theta_1 = \pi$ and $\theta_2 = \pi/2$ the sequence is denoted as half double echo (HDE) RESPDOR. Figure S4 shows numerically simulated heat plots displaying the control signal intensity for HDE RESPDOR and PE REDOR.

Both HDE RESPDOR and PE REDOR are predicted to be less sensitive to MAS frequency deviations than REDOR, however, they are clearly not as robust as DE REDOR.

Figure 2D shows simulated dipolar dephasing difference curves for the various REDOR pulse sequences. The REDOR and DE REDOR dephasing difference curves are identical, showing the exact same rate and extent of dephasing. The HDE RESPDOR curve shows the same extent of dephasing as REDOR, but builds up at exactly half the rate. While the reduction in the rate of dephasing is generally an undesirable feature, it could be useful when very large dipolar coupling constants are to be measured, *i.e.*, the rate of dipolar dephasing can be slowed so that the dipolar oscillations can be more accurately sampled. Additionally, HDE RESPDOR only requires $\pi/2$ pulses on the dephased spin, which is advantageous for nuclei that have a large chemical shift range or for low-γ spins where the accessible RF fields may be limited. PE RESPDOR displays only 70% of the dephasing offered by REDOR and also gives a reduced build-up rate as compared to REDOR or DE REDOR. Finally, PE REDOR shows the same build-up rate, but only half the dephasing as REDOR. However, as described below, the PE REDOR experiments offer improved ^{1}H coherence lifetimes via refocusing of ^{1}H homonuclear dipolar couplings. Hence, in some samples PE REDOR may be the sequence of choice.

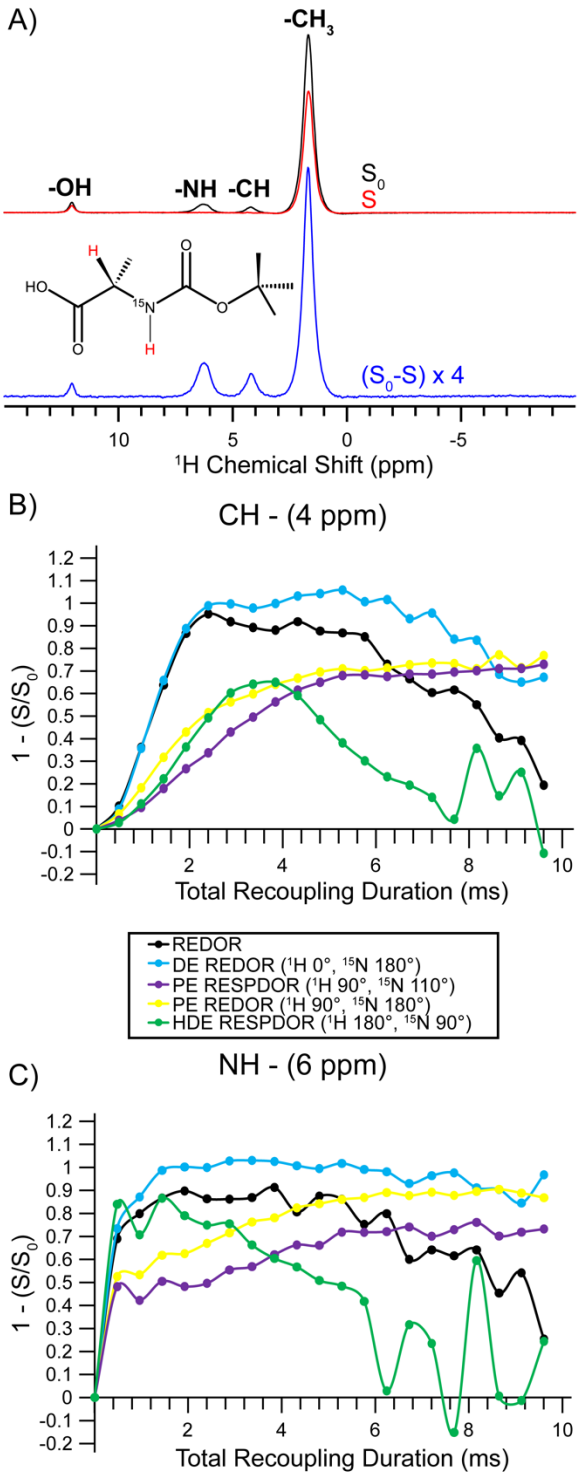

Figure 3. (A) Control (S_0), dephased (S) and difference ($S_0 - S$, intensity scaled by 4) $^{1}H\{^{15}N\}$ DE S-REDOR spectra of TBA obtained with a total recoupling duration 5.28 ms, 64 scans and a 1 s recycle delay. REDOR, DE REDOR, PE RESPDOR, PE REDOR and HDE RESPDOR $\Delta S/S_0$ curves for (B) CH and (C) ^{15}NH sites. In all cases the total $SR4_1^2$ duration was incremented in steps of 0.48 ms.

$^{1}H\{^{15}N\}$ Dipolar Dephasing Experiments. REDOR and RESPDOR $^{1}H\{^{15}N\}$ dipolar dephasing experiments were performed on ^{15}N-labelled t-Butyloxycarbonyl-*L*-alanine (TBA) to test the predictions made by the numerical simulations. For these experiments a 1.3 mm HX probe was employed with a target MAS frequency of 50000 Hz and all pulse durations and timings calculated accordingly. The Bruker MAS III controller typically indicated the MAS frequency fluctuated between 49995 Hz and 50005 Hz. However, this measurement is likely a significant overestimate of the stability of the experimental MAS frequency because the MAS controller averages the frequency over 0.5 s of spinning. Figure 3A shows the control (S_0), dephased (S) and difference ($S_0 - S$) DE REDOR spectra recorded with 5.28 ms of total recoupling. Approximately 32% dephasing is observed for the hydroxyl resonance at 12 ppm, 97% dephasing is observed for the –CH resonance at 4 ppm, 100% dephasing is observed for the amide resonance at 6 ppm, and 34% dephasing was observed for the methyl resonance at 1.5 ppm. As suggested by the simulations shown earlier (Figure 2D), the REDOR and DE REDOR dephasing curves build-up with essentially identical rates and extents of dephasing (Figures 3B and 3C). We focus our subsequent analysis on the CH ^{1}H NMR signal since the ^{1}H-^{15}N dipolar coupling constant is *ca*. 2.5 kHz, resulting in a slower build-up of dephasing than the NH ^{1}H signal and a clearly visible first maximum in the dephasing difference curve.

The experimental $^{1}H\{^{15}N\}$ REDOR $\Delta S/S_0$ curve decreases at longer recoupling times. This contrasts with the DE REDOR dephasing curve, which exhibits a nearly constant intensity even at the longest recoupling times (Figure 3B). As discussed above, the REDOR dephasing curve likely decays at longer recoupling times because the control signal intensity will fluctuate if the MAS is not perfectly stable; on the other hand, the DE REDOR

sequence is predicted to be much more robust to deviations of the MAS frequency. To further illustrate the improved robustness of the DE REDOR sequence, we performed experiments where we varied the MAS frequency entered into the pulse program to calculate pulse timings (Figure S5). In these experiments the experimental MAS frequency and total recoupling duration were fixed at values of 50000 Hz and approximately 3.84 ms, respectively. As expected, the DE REDOR control signal intensity decreases more slowly than REDOR with mis-setting of the input MAS frequency. Figure S5 also shows that the ^{1}H spins with smaller CSA are more tolerant of errors in the pulse timings, while those with larger CSA are less tolerant.

The HDE RESPDOR curve builds-up at half the rate of the REDOR/DE REDOR, in agreement with the simulations. However, the observed dephasing with HDE RESPDOR is only half that observed with REDOR or DE REDOR. The lower than expected experimental dephasing for HDE RESPDOR likely arises because HDE RESPDOR exhibits a similar sensitivity to MAS frequency deviations as REDOR (Figure S4), yet the dephasing builds-up at half the rate, meaning there is practically double the time for errors to accumulate. Therefore, HDE RESPDOR is only suggested for samples where the dipolar coupling constant is very large. As expected from simulations, the extent of dephasing for the PE REDOR and PE RESPDOR is reduced as compared to REDOR, in agreement with the simulations. Interestingly, the PE RESPDOR curves show a continuous build-up of dephasing difference as the recoupling time increases. Indeed, dephasing should continually increase as dipolar couplings to distant ^{15}N spins from adjacent molecules within the lattice are recoupled at longer times. The continuous build-up of dephasing suggests that the PE RESPDOR sequences are very robust to MAS frequency deviations, although simulations

predict the dependence of the control signal intensity on the MAS frequency is intermediate to that of REDOR and DE REDOR (Figure S4). We note that the simulations shown do not account for ^{1}H-^{1}H homonuclear couplings, which pulse sequences with PE symmetry are known to partly refocus.[66]

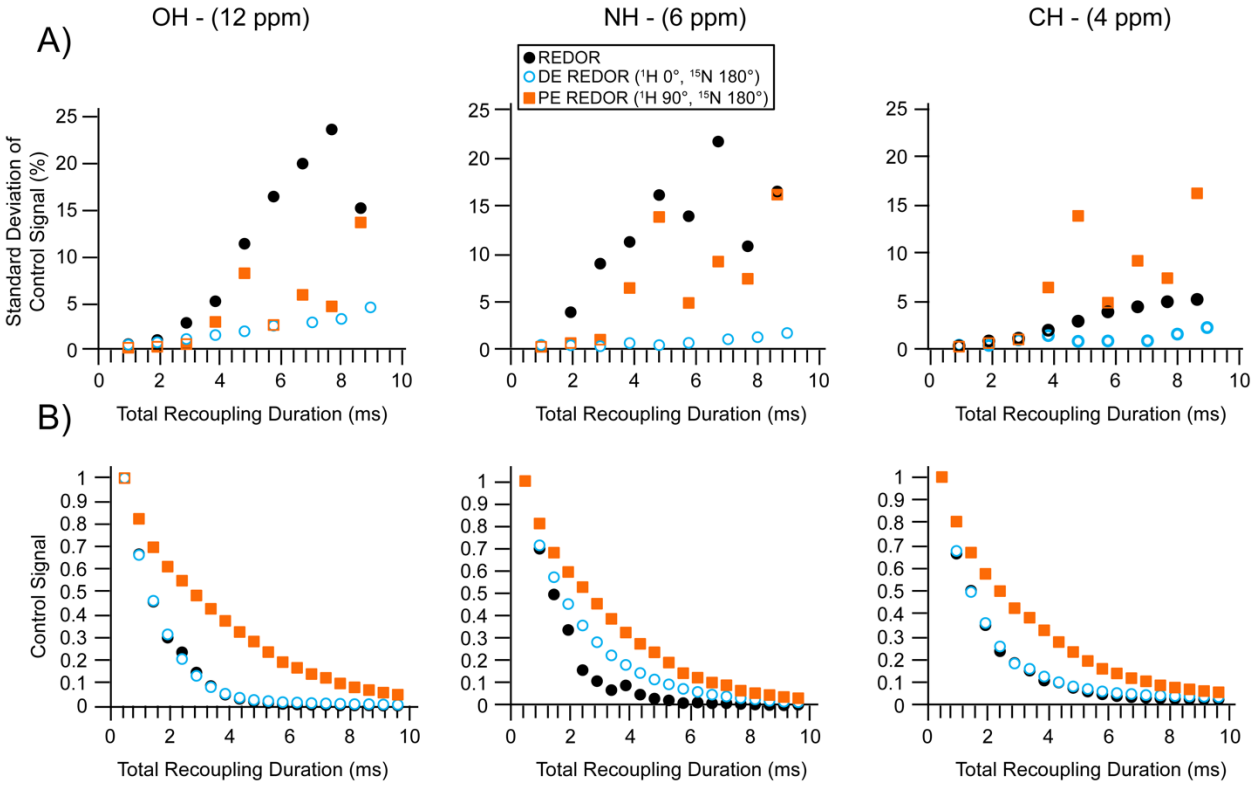

Figure 4. (A) The standard deviation of the REDOR, DE REDOR, and PE REDOR control signal at different recoupling times for the OH, NH and CH ^{1}H NMR signals of TBA. For each recoupling duration, 20 measurements with 64 scans each were performed. (B) The REDOR, DE REDOR, and PE REDOR control signal as a function of recoupling duration.

As was shown with experiments and simulations above, one of the fundamental issues with the REDOR sequence is its susceptibility to MAS frequency variations that causes a loss of signal and decay of dephasing difference curves at long recoupling times. Simulations predicted that the sensitivity to MAS frequency fluctuations becomes worse as the ^{1}H CSA and heteronuclear dipolar coupling increase in magnitude (Figure S1). To further illustrate the

improved robustness of the DE REDOR pulse sequence the normalized standard deviation of the signal intensities was measured for nine different recoupling durations for the –OH, –NH and –CH resonances of TBA (Figure 4A). For each recoupling duration the experiment was repeated twenty times, with 64 scans per point. For a given recoupling duration, each signal intensity was normalized by dividing by the average calculated from the twenty experiments, then the standard deviation was calculated. For all ^{1}H NMR signals, DE REDOR has a significantly lower standard deviation than REDOR and moderately lower standard deviation than PE REDOR, especially at longer recoupling durations where MAS frequency fluctuations will cause variations in the signal intensity. Planewave DFT GIPAW calculations predict the ^{1}H reduced chemical shift anisotropies (δ_{CSA}) of –16.0, –7.3 and –3.1 ppm for the OH, NH and CH, respectively (Table S1). The OH and NH groups exhibit the largest standard deviations, consistent with the SIMPSON simulations shown in Figure 2 and Figure S1 that predict larger ^{1}H CSA and ^{1}H-^{15}N dipolar coupling constants will make the REDOR experiment more sensitive to MAS fluctuations. The large difference in standard deviation between the DE REDOR and REDOR clearly illustrates that the DE REDOR is much more robust.

Figure 4B displays the REDOR, DE REDOR, and PE REDOR control signals plotted as a function of the total recoupling duration. For the CH and OH ^{1}H resonances, the DE REDOR control signal intensity decreases at a similar rate as the REDOR signal. Although, for the NH ^{1}H resonance, the DE REDOR control signal decreases slightly more slowly than REDOR, likely due to better refocusing of ^{1}H CSA and heteronuclear dipolar couplings when the experimental MAS frequency deviates from its ideal value. In all cases the PE REDOR control signal intensity decreases more slowly with respect to the total recoupling duration than REDOR and DE REDOR.

We further tested the DE REDOR sequence on TBA with experiments at 14.1 T to observe the effects of the increasing magnetic field on scaling of the ^{1}H CSA (Figure S6). Note that these experiments employed a MAS controller from Phoenix NMR Inc., which indicated that the spinning frequency varied between 49985 Hz and 50015 Hz, however, the Phoenix MAS controller updates the MAS frequency every 0.25 s, implying that there is less averaging in the displayed MAS frequencies. Hence, we believe that the true fluctuations in the MAS frequency are comparable for the 9.4 T and 14.1 T experiments. The REDOR and DE REDOR $\Delta S/S_0$ curves obtained at 14.1 T are similar to those obtained at 9.4 T, with the REDOR curves exhibiting significant fluctuations at longer recoupling times.

Measurement of ^{1}H-^{15}N dipolar coupling constants and N-H internuclear distances. The ^{15}N-^{1}H dipolar coupling constants and intramolecular internuclear distances were extracted for the CH and NH ^{1}H spins of TBA by using SIMPSON to calculate $\Delta S/S_0$ curves for DE REDOR or REDOR, respectively (Figure S7). Comparison of the experimental CH ^{1}H{^{15}N} DE REDOR dipolar dephasing curves with simulations suggests that the d_{NH} is 1.4 kHz, corresponding to a CH--N intramolecular distance of 2.06 Å, in good agreement with the distance of 2.08 Å obtained from the known crystal structure of TBA,[76] after plane-wave DFT optimization of the hydrogen atom positions. For the NH bond length measurement, the ^{1}H{^{15}N} REDOR $\Delta S/S_0$ curve was used for distance measurement. REDOR allows the total recoupling duration to be stepped in increments of 80 μs, whereas DE REDOR requires minimum increments of 160 μs (for a 50 kHz MAS frequency with $SR4_1^2$ recoupling). Therefore, REDOR allows a finer sampling of the initial part of the dipolar dephasing curve. Fits of the experimental ^{1}H{^{15}N} REDOR curve yield d_{NH} = 12500

kHz, corresponding to a NH distance of 0.99 Å (Figure S7). This distance is in reasonable agreement with the value of 1.02 Å observed in the DFT-optimized crystal structure. Because REDOR and DE REDOR dephasing difference curves build-up at nearly identical rates and the minimum increment size of the total recoupling duration of DE REDOR (160 μs) is twice that of REDOR (80 μs), it could be possible to use REDOR for acquisition of initial parts of the dephasing difference curve and DE REDOR for the second part, but this strategy was not tested here.

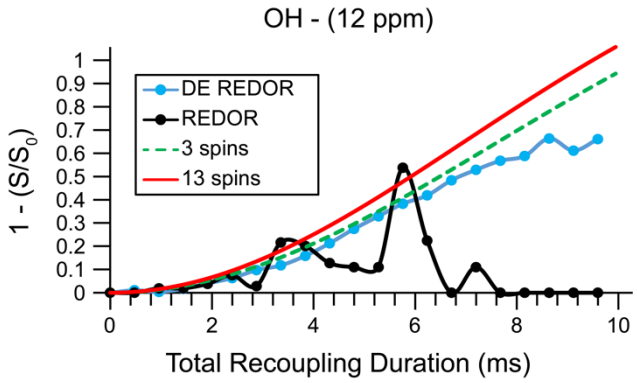

Figure 5. $^{1}H\{^{15}N\}$ REDOR (black) and DE REDOR (blue) dephasing difference curves for the OH ^{1}H NMR signal of TBA (points). Corresponding 3-spin (green dashed line) and 13-spin simulations (red solid line) are shown as solid lines.

Figure 5 shows the $^{1}H\{^{15}N\}$ REDOR and DE REDOR dephasing difference curves for the OH ^{1}H of TBA. Analysis of these curves is challenging because the crystal structure of TBA shows that there are two similar internuclear distances between the OH and nitrogen atoms.[76] These distances are predicted to be 4.38 Å (intermolecular) and 4.40 Å (intermolecular) which correspond to d_{NH} of 145 Hz and 143 Hz, respectively. Additionally, there are 4 other nitrogen atoms within distances of 5.475 Å (d_{NH} = 74 Hz) and 6.83 Å (d_{NH} = 38 Hz). Since all ^{1}H-^{15}N dipolar coupling constants are relatively weak for the OH hydrogen, recoupling durations longer than 2 ms are required to observe significant dipolar dephasing. However, the $^{1}H\{^{15}N\}$ REDOR

$\Delta S/S_0$ curve shows large amplitude variations at recoupling times longer than 4 ms, likely because the OH hydrogen are predicted to have significant ^{1}H CSA (δ_{CSA} = –16 ppm from GIPAW DFT calculations). The DE REDOR $\Delta S/S_0$ curve is clearly much more stable than the REDOR one.

Simulated $\Delta S/S_0$ curves were obtained using either the two nearest or twelve nearest ^{15}N internuclear distances in the optimized crystal structure and accounting for the relative orientations of the NH internuclear vectors, as has been previously described.[77,78] In both cases the experimental dephasing difference is slightly below that predicted by the multi-spin simulations. We note that the experimental dephasing difference curves for CH and OH also show lower than expected dephasing at recoupling durations longer than 5 ms (Figure 3). Therefore, the discrepancy between the fit and the experimental DE REDOR $\Delta S/S_0$ curve likely reflects a slight reduction in the experimental dephasing difference at longer recoupling durations.

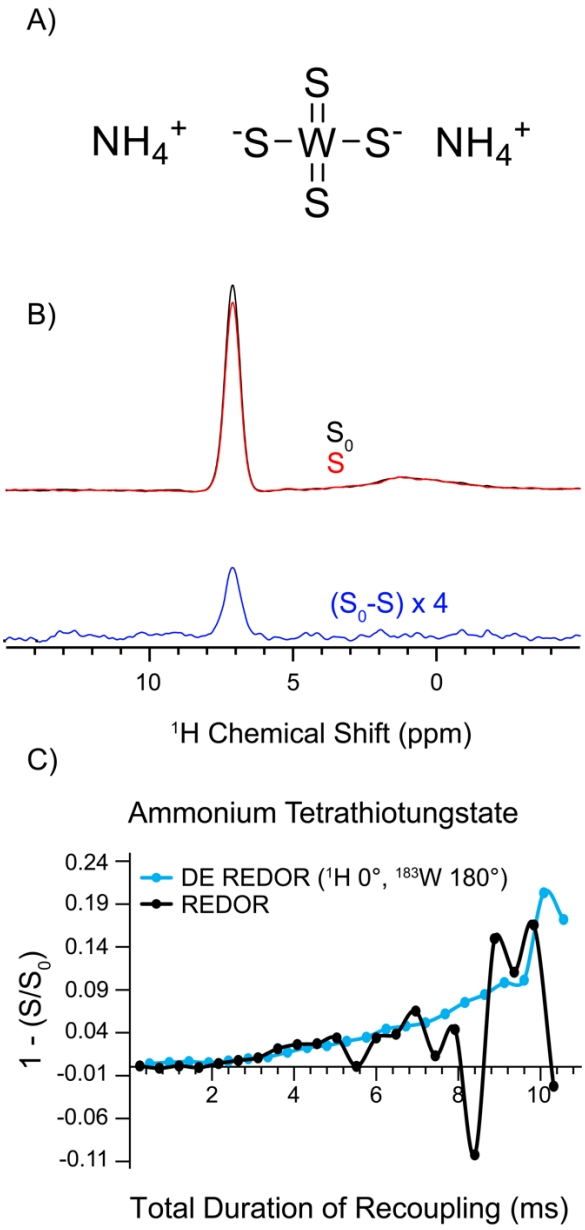

Figure 6. (A) Structure of ammonium tetrathiotungstate. (B) Control (S_0), dephased (S) and difference ($S_0 - S$) spectrum of ammonium tetrathiotungstate. Spectra were recorded with a dipolar recoupling time of 8.64 ms, 64 scans, and a 1 s recycle delay. (C) ^{1}H{^{183}W} dipolar dephasing curves recorded with REDOR and DE REDOR pulse sequences. All experiments were performed with a 50 kHz MAS frequency.

$^{1}H\{^{183}W\}$ DE S-REDOR. The various ^{1}H detected REDOR pulse sequences were also tested to observe dipolar dephasing caused by unreceptive nuclei. First, we used ammonium tetrathiotungstate, $(NH_4)_2WS_4$, to perform ^{1}H{^{183}W} REDOR experiments (Figure 6A). Ammonium tetrathiotungstate is a common standard for setup of ^{1}H-^{183}W CPMAS

experiments.[54,79] ^{183}W is a spin-1/2 nucleus with an extremely low gyromagnetic ratio ($\frac{\omega_0}{2\pi}$= 16.66 MHz at 9.4 T) and moderate natural isotopic abundance of 14.4%. This particular sample also features weak ^{1}H-^{183}W dipolar coupling constants which are likely less than 160 Hz. The dipolar coupling constants are small because of the low gyromagnetic ratio of ^{183}W and the significant ^{1}H-^{183}W internuclear distances > 3 Å. Consequently, ^{1}H detection of ^{183}W dipolar dephasing is extremely challenging because dipolar recoupling durations longer than 6 ms are required to generate appreciable dephasing. However, the use of conventional ^{1}H{^{183}W} REDOR results in an unreliable dephasing difference curve that shows random fluctuations at longer recoupling durations. On the other hand, with the DE REDOR pulse sequence the difference curve shows a smoother build-up as the recoupling duration is increased. Consequently, a reliable DE REDOR difference spectrum can be obtained (Figure 6B). Note, this curve was not fit since the dephasing will result from many ^{1}H-^{183}W spin pairs within the lattice. Furthermore, the ammonium ions may exhibit dynamic reorientation in the solid-state, further complicating analysis.

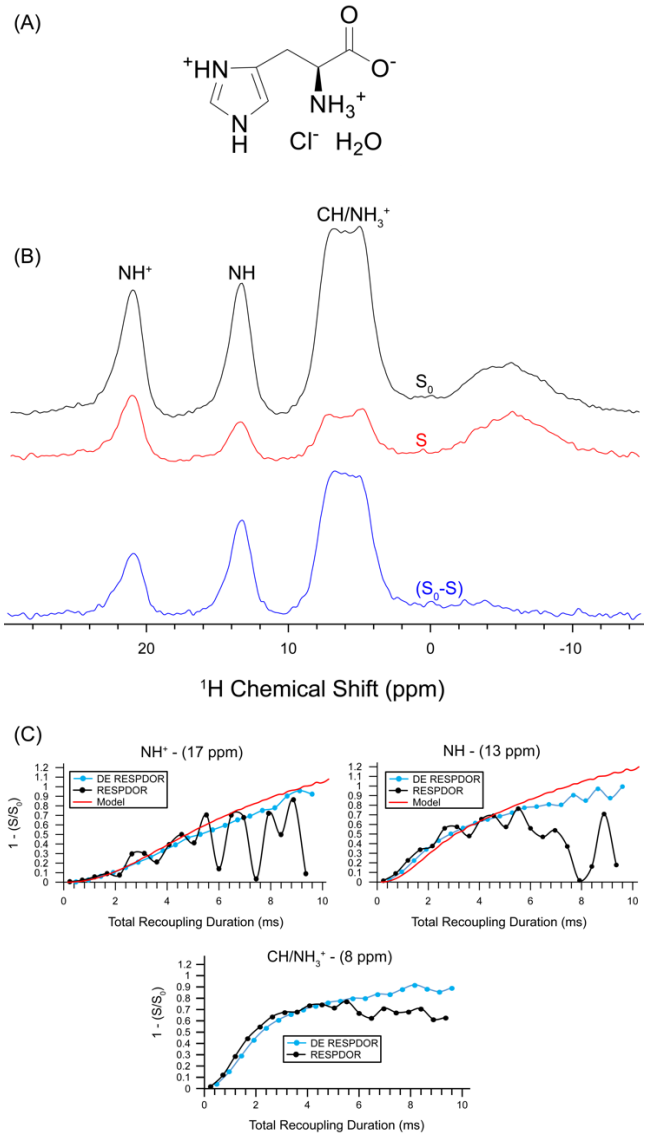

Figure 7. (A) Structure of histidine•HCl•H_2O (histidine). (B) Control (S_0), dephased (S) and difference ($S_0 - S$) $^1H\{^{35}Cl\}$ NMR spectra of histidine obtained with DE RESPDOR. Spectra were recorded with a total dipolar recoupling duration of 5.28 ms, 64 scans and a 2 s recycle delay. (C) $^1H\{^{35}Cl\}$ ΔS curves recorded with DE S-RESPDOR and S-RESPDOR pulse sequences for NH^+ (17 ppm), NH (12 ppm) and CH/NH_3^+ (8 ppm) ^1H NMR signals. All experiments were performed with a 50 kHz MAS frequency. Multi-spin simulations (red lines) are shown for the NH and NH^+ $^1H\{^{35}Cl\}$ DE S-RESPDOR $\Delta S/S_0$ curves.

$^1H\{^{35}Cl\}$ S-RESPDOR Experiments. Histidine•HCl•H_2O contains ^{35}Cl, which is a spin-3/2 quadrupolar nucleus with a low gyromagnetic ratio ($\frac{\omega_0}{2\pi}$= 39.24 MHz at 9.4 T) and natural isotopic abundance of 75.78%. We note that ^{35}Cl solid-state NMR spectroscopy has been used to

probe the structure of a variety of amino acid and pharmaceutical hydrochloride salts.[80,81] ^{1}H detected ^{35}Cl solid-state NMR spectra of hydrochloride salts have previously been obtained with D-RINEPT and HMQC pulse sequences.[63,66,82-84] From this point forward, histidine•HCl•H_2O is simply referred to as histidine. The ^{35}Cl nuclei within histidine experience a sizable second-order quadrupolar interactions (C_Q = 1.95 MHz),[63] consequently, 30 μs saturation pulses (1.5 rotor cycle duration) were applied on the ^{35}Cl channel to induce dephasing.[68] The radiofrequency of the ^{35}Cl saturation pulses was 50 kHz and was experimentally optimized to maximize dephasing. We note that numerical simulations predict that the extent and rate of dipolar dephasing is comparable for both RESPDOR and DE RESPDOR when the saturation pulses have similar RF field (simulations are also shown for ^{14}N, Figure S8).

The ^{1}H{^{35}Cl} RESPDOR and DE RESPDOR dephasing curves are plotted in Figure 7C for NH^+ (17 ppm), NH (12 ppm) and CH/NH_3^+ (8 ppm) ^{1}H NMR signals of histidine. Note that the imidazolium CH ^{1}H NMR signals partly overlap with the ammonium NH_3^+ ^{1}H NMR signals which reduces the apparent extent of dephasing. Inspection of the ^{1}H{^{35}Cl} RESPDOR and DE RESPDOR curves shows that both have similar build-up rates for all ^{1}H NMR signals. For the NH_3^+ ^{1}H NMR signal the ^{1}H{^{35}Cl} RESPDOR and DE RESPDOR dephasing curves are nearly identical. However, the RESPDOR $\Delta S/S_0$ curves for NH and NH^+ ^{1}H NMR signals show significant random fluctuations after 2 ms recoupling. Only with the DE RESPDOR pulse sequence is it possible to obtain reliable $\Delta S/S_0$ curves at recoupling times longer than 4 ms. We note that planewave DFT GIPAW calculations predict large ^{1}H δ_{CSA} of –16.8 and –9.0 ppm for the NH^+ and NH, respectively. In addition, each of these ^{1}H spins will have sizeable ^{1}H-^{14}N heteronuclear dipolar coupling constants on the order of 10 kHz. Indeed simulations including ^{1}H-^{14}N heteronuclear dipolar couplings show that the control signal becomes more sensitive to

MAS frequency fluctuations (Figure S10). Therefore, it is expected that these two ^{1}H signals will be very sensitive to MAS frequency fluctuations. We note that a ^{1}H δ_{CSA} of –16.4 ppm is predicted for NH_3^+, however, rapid rotation of the NH_3^+ group partly averages the ^{1}H CSA and heteronuclear dipolar couplings to ^{14}N, explaining why the REDOR dephasing curve does not fluctuate or decay at longer recoupling times.

Inspection of the crystal structure shows that each hydrogen atom has several chloride anions within a radius of 6 Å (see Figure S9 and Table S2). The crystal structure indicates that two of the H atoms of the NH_3^+ group make contacts of 2.17 and 2.27 Å that correspond to ^{1}H-^{35}Cl dipolar coupling constants of 1153 Hz and 1007 Hz, respectively. The imidazolium CH have nearest Cl distances of 2.42 Å and 2.75 Å that correspond to dipolar coupling constants of 831 Hz and 567 Hz. Fitting of this curve was not attempted given the overlap of imidazolium CH and NH_3^+ ^{1}H signals, the presence of multiple H-Cl distances, and the rotation of the NH_3^+ group that will partly average the H-Cl distances and ^{1}H-^{35}Cl dipolar coupling constants. The closest H-Cl distance for the NH is 2.96 Å which corresponds to a dipolar coupling constant of 454 Hz and there are second and third nearest neighbors at distances of 4.21 Å (d = 158 Hz) and 4.42 Å (d = 136 Hz). The closest H-Cl distance for the NH^+ ^{1}H is 3.88 Å which corresponds to a dipolar coupling constant of 202 Hz, with other nearest neighbors at distances of 4.40 Å (d = 138 Hz) and 4.53 Å (d = 127 Hz). Consistent with the trends in H-Cl inter-nuclear distances, the dephasing difference curves for CH/NH^{3+} and NH show a faster buildup than the NH^+ curve.

Modeling of the ^{1}H{^{35}Cl} DE RESPDOR dephasing difference curves is challenging because a large number of Cl atoms must be considered and furthermore, multiple spin-systems need to be used because the natural isotopic abundance of ^{35}Cl is below 100%. To model the NH^+ and NH $\Delta S/S_0$ curves we considered the H-Cl distances within the known single crystal

neutron diffraction structure of histidine (after DFT optimization of H atom positions).[85] Briefly, 2-spin (^{1}H-^{35}Cl), 3-spin (^{1}H-^{35}Cl-^{35}Cl) and 4-spin (^{1}H-^{35}Cl-^{35}Cl-^{35}Cl) numerical SIMPSON simulations were used to model the dephasing curves for the three nearest Cl atoms (^{35}Cl homonuclear dipolar coupling was neglected). Each of these curves were summed together with a weighting calculated from the probability of each spin-system occurring based upon the natural isotopic abundance of ^{35}Cl (see Table S2). In addition, the dephasing from all other ^{35}Cl spins was accounted for by calculating a 2-spin dephasing curve with a single effective ^{1}H-^{35}Cl dipolar coupling constant (the heterodipolar second moment).[86-88] The effective dipolar coupling constant (d_{eff}) was calculated from the square root square sum of all ^{1}H-^{35}Cl dipolar coupling constants for all Cl atoms within *ca*. 25 Å of each H atom (excluding the three nearest Cl atoms which were already explicitly modeled). For this step, 24.22% of the Cl atoms were randomly removed to account for the 75.78% NA of ^{35}Cl. The procedure described above results in simulated $\Delta S/S_0$ curves which show reasonable agreement with the experimental ones (Figure 7C). However, there are deviations visible between the simulated and experimental curves. At longer recoupling durations the experimental curve lies below the simulated curve, consistent with the other experimental results throughout the manuscript. But, for the NH curve, the initial dephasing is slightly underestimated.

Conclusion

In conclusion several double echo S-REDOR and S-RESPDOR pulse sequences were described. The double echo pulse sequences provide a much more reliable observation of ^{1}H detected dipolar dephasing, enabling ^{1}H detected measurements of heteronuclear dipolar

coupling constants, even when the dipolar coupling constants are on the order of *ca.* 100 Hz. These pulse sequences should also be useful for spectral editing experiments with a variety of unreceptive spin-1/2 and quadrupolar nuclei. Through both numerical simulations and experiments the double echo family of sequences was shown to be much more robust than the corresponding S-REDOR/S-RESPDOR pulse sequences. Consistent with prior literature, experimental S-REDOR/S-RESPDOR curves showed a decay of the dephasing difference signal at recoupling durations longer than several milliseconds. This decay was attributed to a decrease in the control signal that occurs because experimental fluctuations of the MAS frequency by a few Hz leads to imperfect refocusing of ^{1}H CSA and heteronuclear dipolar coupling constants. The double echo sequences were shown to provide nearly identical dephasing curves to those obtained with conventional REDOR/RESPDOR sequences, except dephasing could be observed out to longer recoupling times. Therefore, we recommend that the DE REDOR/DE RESPDOR sequences be used in place of the conventional sequences as they provide a more reliable measurement of dipolar dephasing. In systems with significant homonuclear couplings perfect echo REDOR sequences may be of interest. Finally, the half double echo RESPDOR sequence may be useful for systems with large heteronuclear dipolar interactions because it provides half the dephasing rate as REDOR or DE REDOR.

We anticipate that the double echo sequences will be especially beneficial for experiments at higher static magnetic fields since the ^{1}H CSA will scale with the strength of the applied field. The DE sequences should also prove useful for experiments with faster MAS frequencies greater than 50 kHz. For example, 100 kHz MAS experiments are now becoming commonplace.[44] In the presence of unstable MAS, an increase in MAS frequency will lead to the accumulation of more errors, therefore, we expect that the DE REDOR family of pulse

sequences will be especially beneficial. Further experiments are required to test all of these hypotheses. Finally, in a forthcoming manuscript we will also demonstrate that low-power, long-duration saturation pulses can be incorporated into $^{1}H\{^{195}Pt\}$ DE RESPDOR experiments. By varying the offset of the saturation pulses it is possible to reconstruct the entire ^{195}Pt MAS spectrum. This approach enables rapid indirectly detection of ^{195}Pt MAS solid-state NMR spectra and allows measurement of CS tensor parameters.

Experimental

Solid-State NMR Spectroscopy Experiments. All experiments, except those shown in Figure S3, were performed with a 9.4 T wide-bore magnet equipped with a Bruker Avance III HD console and 1.3 mm Bruker HX probe. A shunt capacitor was inserted in parallel with the primary variable tuning capacitor of the X channel to tune to ^{183}W (ν_0 (^{183}W) = 16.67 MHz). Additional $^{1}H\{^{15}N\}$ REDOR experiments were performed with a 14.1 T widebore NMR magnet equipped with a Bruker Avance NEO HD console and a 1.3 mm Phoenix HXY probe configured in double resonance mode.

All samples were handled under ambient conditions and packed into 1.3 mm zirconia rotors that were spun using N_2 gas for NMR experiments at 9.4 T; compressed air was used for spinning at 14.1 T. ^{1}H chemical shifts were indirectly referenced to neat tetramethylsilane by using adamantane (δ_{iso} (^{1}H) = 1.82 ppm). The ^{1}H RF powers were calibrated directly on each sample by using a $\pi/2$-spin-lock pulse sequence by determining the second-order rotary resonance recoupling condition, (R^3, $\nu_1 = 2 \times \nu_{rot}$). A 100 kHz RF field was used for all ^{1}H pulses. All S-REDOR/S-RESPDOR experiments utilized $SR4_1^2$ dipolar recoupling on the ^{1}H channel.[29] The DE REDOR/RESPDOR pulse sequence employed a 64 step phase cycle, while

conventional REDOR pulse sequence used a 32 step phase cycle. Pulse sequences compatible with Bruker Avance III spectrometers have been provided as Supplementary Material.

^{15}N-enriched TBA was used as received from CDN Isotopes. All experiments were performed at 50 kHz MAS. The ^{1}H{^{15}N} REDOR curves were acquired with a 1.48 s recycle delay (the ^{1}H T_1 is about 1.14 s), 64 scans, and 120 recoupling increments with the duration of $SR4_1^2$ recoupling incremented in steps of 80 μs. The DE REDOR, HDE RESPDOR, and PE RESPDOR dephasing curves were acquired with a 1 s recycle delay, 64 scans, and 60 recoupling increments, with the duration of $SR4_1^2$ incremented in steps of 80 μs (for individual $R4_1^2$ cycles) or 240 μs (for complete supercycles). The ^{15}N π/2 and π pulse durations were 2.55 μs and 5.1 μs, respectively.

Histidine•HCl•H_2O was used as received from Fluka. All experiments were performed at 50 kHz MAS at 9.4 T. The ^{1}H{^{35}Cl} RESPDOR curves were acquired with a 4 s recycle delay (^{1}H T_1 is approximately 2.9 s), 16 scans, and 20 recoupling increments with the duration of $SR4_1^2$ incremented in steps of 480 μs. The DE RESPDOR dephasing curves were acquired with a 2 s recycle delay, 64 scans, and 22 recoupling increments with the duration of $SR4_1^2$ recoupling incremented in steps of 480 μs. All ^{35}Cl RESPDOR experiments employed a 30 μs saturation pulse ($1.5 \times \nu_{rot}$) with a 50 kHz RF field. The power for ^{35}Cl saturation pulses was optimized to give maximum dephasing of the ^{1}H signal. Since the Larmour frequency of ^{15}N is close to that of ^{35}Cl, (ν_0(^{15}N) = 40.56 MHz) and (ν_0(^{35}Cl) = 39.24 MHz), the ^{35}Cl RF field was calibrated on ^{15}N.

Ammonium tetrathiotungstate was used as received from Sigma-Aldrich. All experiments were performed at 50 kHz MAS at 9.4 T. The ^{1}H{^{183}W} REDOR curves were acquired with a 5 s recycle delay (^{1}H T_1 is about 17 s) 32 scans, and 22 recoupling increments with the duration of

$SR4_1^2$ recoupling incremented in steps of 480 μs. The DE REDOR curves were acquired with a 5 s recycle delay, 64 scans, and 22 recoupling increments with the duration of $SR4_1^2$ recoupling incremented in steps of 480 μs. All ^{183}W π/2 and π pulses were 5.5 μs and 11 μs, respectively.

Numerical Simulations. Numerical simulations were performed using SIMPSON v4.1.1.[89-91] The SIMPSON input code is provided in the Supplementary Material. All pulses in the files were of finite duration, except the initial ^{1}H π/2 pulses, which were ideal. The rep320 crystal file was used to simulate all dephasing curves, and the rep30 crystal was used to simulate 2D heat plots. The number of gamma angles in both cases was 13. For calculations of heat plots, the MAS frequency was varied systematically from 49970 Hz to 50030 Hz in steps of 1 Hz. Heat plots were constructed using MATLAB_R2015B. The MATLAB script for the calculation of S, S_0 and ΔS curves with variation of the MAS frequency has been included as Supplementary Material. The rep320 crystal file with 17 gamma angles was used for simulations of ^{1}H{^{35}Cl} dipolar dephasing difference curves.

Planewave-DFT calculations on TBA and histidine were performed using CASTEP[92] with the PBE-GGA functional,[93] TS dispersion correction scheme[94] and ultra-soft pseudopotentials.[95,96] Hydrogen atom positions were optimized prior to performing the NMR calculations. The GIPAW method was used to calculate the magnetic shielding tensors.[97] A 630 eV kinetic cutoff energy and k-point spacing of 0.07 Å^{-1} was used for the Monkhorst–Pack grid for all calculations.

Supplementary Material Available

The Supplementary material shows additional figures summarizing NMR experiments and simulations as well as SIMPSON code inputs. Bruker pulse programs, MATLAB scripts, and raw NMR data for main text and Supplementary figures are available for download at https://doi.org/10.5281/zenodo.5745945.

Acknowledgements

Solid-state NMR experiments and data analysis were supported by the U.S. Department of Energy (DOE), Office of Science, Basic Energy Sciences, Materials Science and Engineering Division. The Ames Laboratory is operated for the U.S. DOE by Iowa State University under Contract DE-AC02-07CH11358. A.J.R. acknowledges additional support from the Alfred P. Sloan Foundation through a Sloan research fellowship.

References:

(1) Reif, B.; Ashbrook, S. E.; Emsley, L.; Hong, M. *Nature Reviews Methods Primers* **2021**, *1*, 2.
(2) Brown, S. P.; Spiess, H. W. *Chem. Rev.* **2001**, *101*, 4125-4155.
(3) Chien, P.-H.; Griffith, K. J.; Liu, H.; Gan, Z.; Hu, Y.-Y. *Annual Review of Materials Research* **2020**, *50*, 493-520.
(4) Jaroniec, C. P.; MacPhee, C. E.; Bajaj, V. S.; McMahon, M. T.; Dobson, C. M.; Griffin, R. G. *Proceedings of the National Academy of Sciences of the United States of America* **2004**, *101*, 711.
(5) Brouwer, D. H.; Kristiansen, P. E.; Fyfe, C. A.; Levitt, M. H. *J. Am. Chem. Soc.* **2005**, *127*, 542-543.
(6) Bajaj, V. S.; Mak-Jurkauskas, M. L.; Belenky, M.; Herzfeld, J.; Griffin, R. G. *J. Magn. Reson.* **2010**, *202*, 9-13.
(7) Cady, S. D.; Schmidt-Rohr, K.; Wang, J.; Soto, C. S.; DeGrado, W. F.; Hong, M. *Nature* **2010**, *463*, 689-692.
(8) Hu, Y. Y.; Rawal, A.; Schmidt-Rohr, K. *Proceedings of the National Academy of Sciences* **2010**, *107*, 22425.
(9) Haimovich, A.; Eliav, U.; Goldbourt, A. *J. Am. Chem. Soc.* **2012**, *134*, 5647-5651.
(10) Kong, X.; Deng, H.; Yan, F.; Kim, J.; Swisher, J. A.; Smit, B.; Yaghi, O. M.; Reimer, J. A. *Science* **2013**, *341*, 882.
(11) Perras Frédéric, A.; Wang, Z.; Naik, P.; Slowing Igor, I.; Pruski, M. *Angewandte Chemie International Edition* **2017**, *56*, 9165-9169.
(12) Berruyer, P.; Lelli, M.; Conley, M. P.; Silverio, D. L.; Widdifield, C. M.; Siddiqi, G.; Gajan, D.; Lesage, A.; Coperet, C.; Emsley, L. *J. Am. Chem. Soc.* **2017**, *139*, 849-855.
(13) Cegelski, L. *Bioorganic & Medicinal Chemistry Letters* **2013**, *23*, 5767-5775.
(14) Duong, N. T.; Aoyama, Y.; Kawamoto, K.; Yamazaki, T.; Nishiyama, Y. *Molecules* **2021**, *26*.
(15) Perras, F. A.; Kanbur, U.; Paterson, A. L.; Chatterjee, P.; Slowing, I. I.; Sadow, A. D. *Inorg. Chem.* **2021**.
(16) Zhao, X.; Sudmeier, J. L.; Bachovchin, W. W.; Levitt, M. H. *J. Am. Chem. Soc.* **2001**, *123*, 11097-11098.
(17) Franks, W. T.; Zhou, D. H.; Wylie, B. J.; Money, B. G.; Graesser, D. T.; Frericks, H. L.; Sahota, G.; Rienstra, C. M. *J. Am. Chem. Soc.* **2005**, *127*, 12291-12305.
(18) Lorieau, J. L.; McDermott, A. E. *J. Am. Chem. Soc.* **2006**, *128*, 11505-11512.

(19) Perras, F. A.; Kobayashi, T.; Pruski, M. *J. Am. Chem. Soc.* **2015**, *137*, 8336–8339.
(20) Schanda, P.; Ernst, M. *Prog. Nucl. Magn. Reson. Spectrosc.* **2016**, *96*, 1-46.
(21) Blanc, F.; Basset, J. M.; Coperet, C.; Sinha, A.; Tonzetich, Z. J.; Schrock, R. R.; Solans-Monfort, X.; Clot, E.; Eisenstein, O.; Lesage, A.; Emsley, L. *J. Am. Chem. Soc.* **2008**, *130*, 5886-5900.
(22) Chen, Q.; Schmidt-Rohr, K. *Macromol. Chem. Phys.* **2007**, *208*, 2189-2203.
(23) Munowitz, M. G.; Griffin, R. G.; Bodenhausen, G.; Huang, T. H. *J. Am. Chem. Soc.* **1981**, *103*, 2529-2533.
(24) Gullion, T.; Schaefer, J. *J. Magn. Reson.* **1989**, *81*, 196-200.
(25) Pan, Y.; Gullion, T.; Schaefer, J. *J. Magn. Reson.* **1990**, *90*, 330-340.
(26) Wu, C. H.; Ramamoorthy, A.; Opella, S. J. *J. Magn. Reson., Ser A* **1994**, *109*, 270-272.
(27) Hong, M.; Gross, J. D.; Rienstra, C. M.; Griffin, R. G.; Kumashiro, K. K.; Schmidt-Rohr, K. *J. Magn. Reson.* **1997**, *129*, 85-92.
(28) van Rossum, B. J.; de Groot, C. P.; Ladizhansky, V.; Vega, S.; de Groot, H. J. M. *J. Am. Chem. Soc.* **2000**, *122*, 3465-3472.
(29) Brinkmann, A.; Kentgens, A. P. M. *J. Am. Chem. Soc.* **2006**, *128*, 14758-14759.
(30) Dvinskikh, S. V.; Zimmermann, H.; Maliniak, A.; Sandström, D. *J. Magn. Reson.* **2004**, *168*, 194-201.
(31) Gan, Z. *J. Magn. Reson.* **2006**, *183*, 235-241.
(32) Levitt, M. H. *eMagRes* **2007**.
(33) Nimerovsky, E.; Goldbourt, A. *J. Magn. Reson.* **2010**, *206*, 52-58.
(34) Chen, L.; Wang, Q.; Hu, B.; Lafon, O.; Trébosc, J.; Deng, F.; Amoureux, J.-P. *Phys. Chem. Chem. Phys.* **2010**, *12*, 9395-9405.
(35) Duong, N. T.; Raran-Kurussi, S.; Nishiyama, Y.; Agarwal, V. *J. Phys. Chem. Lett.* **2018**, *9*, 5948-5954.
(36) Schnell, I. *Prog. Nucl. Magn. Reson. Spectrosc.* **2004**, *45*, 145-207.
(37) Dusold, S.; Sebald, A. In *Annual Reports on NMR Spectroscopy*; Academic Press: 2000; Vol. 41, p 185-264.
(38) De Paëpe, G. *Annu. Rev. Phys. Chem.* **2012**, *63*, 661-684.
(39) Ji, Y.; Liang, L.; Bao, X.; Hou, G. *Solid State Nucl. Magn. Reson.* **2021**, *112*, 101711.
(40) Goldbourt, A. *Magn. Reson. Chem.* **2021**, *59*, 908-919.
(41) Ishii, Y.; Tycko, R. *J. Magn. Reson.* **2000**, *142*, 199-204.
(42) Samoson, A.; Tuherm, T.; Gan, Z. *Solid State Nucl. Magn. Reson.* **2001**, *20*, 130-136.
(43) Schnell, I.; Spiess, H. W. *J. Magn. Reson.* **2001**, *151*, 153-227.
(44) Nishiyama, Y. *Solid State Nucl. Magn. Reson.* **2016**, *78*, 24-36.
(45) Wiench, J. W.; Bronnimann, C. E.; Lin, V. S. Y.; Pruski, M. *J. Am. Chem. Soc.* **2007**, *129*, 12076-12077.
(46) Zhou, D. H.; Shah, G.; Cormos, M.; Mullen, C.; Sandoz, D.; Rienstra, C. M. *J. Am. Chem. Soc.* **2007**, *129*, 11791-11801.
(47) Rossini, A. J.; Hanrahan, M. P.; Thuo, M. *Phys. Chem. Chem. Phys.* **2016**, *18*, 25284-25295.
(48) Venkatesh, A.; Lund, A.; Rochlitz, L.; Jabbour, R.; Gordon, C. P.; Menzildjian, G.; Viger-Gravel, J.; Berruyer, P.; Gajan, D.; Copéret, C.; Lesage, A.; Rossini, A. J. *J. Am. Chem. Soc.* **2020**, *142*, 18936-18945.
(49) Venkatesh, A.; Perras, F. A.; Rossini, A. J. *J. Magn. Reson.* **2021**, *327*, 106983.

(50) Hanrahan, M. P.; Men, L.; Rosales, B. A.; Vela, J.; Rossini, A. J. *Chem. Mater.* **2018**, *30*, 7005-7015.
(51) Chen, Y.; Smock, S. R.; Flintgruber, A. H.; Perras, F. A.; Brutchey, R. L.; Rossini, A. J. *J. Am. Chem. Soc.* **2020**, *142*, 6117-6127.
(52) Wang, Z.; Hanrahan, M. P.; Kobayashi, T.; Perras, F. A.; Chen, Y.; Engelke, F.; Reiter, C.; Purea, A.; Rossini, A. J.; Pruski, M. *Solid State Nucl. Magn. Reson.* **2020**, *109*, 101685.
(53) Venkatesh, A.; Hung, I.; Boteju, K. C.; Sadow, A. D.; Gor'kov, P. L.; Gan, Z.; Rossini, A. J. *Solid State Nucl. Magn. Reson.* **2020**, *105*, 101636.
(54) Venkatesh, A.; Ryan, M. J.; Biswas, A.; Boteju, K. C.; Sadow, A. D.; Rossini, A. J. *The Journal of Physical Chemistry A* **2018**, *122*, 5635-5643.
(55) Grey, C. P.; Vega, A. *J. Am. Chem. Soc.* **1995**, *117*, 8232-8242
(56) Goldbourt, A.; Vega, S.; Gullion, T.; Vega, A. J. *J. Am. Chem. Soc.* **2003**, *125*, 11194-11195.
(57) Gan, Z. H. *J. Am. Chem. Soc.* **2006**, *128*, 6040-6041.
(58) Gan, Z. H. *Chemical Communications* **2006**, 4712-4714.
(59) Cavadini, S.; Antonijevic, S.; Lupulescu, A.; Bodenhausen, G. *ChemPhysChem* **2007**, *8*, 1363-1374.
(60) Lafon, O.; Wang, Q.; Hu, B. W.; Vasconcelos, F.; Trebosc, J.; Cristol, S.; Deng, F.; Amoureux, J. P. *J. Phys. Chem. A* **2009**, *113*, 12864-12878.
(61) Nishiyama, Y.; Endo, Y.; Nemoto, T.; Utsumi, H.; Yamauchi, K.; Hioka, K.; Asakura, T. *J. Magn. Reson.* **2011**, *208*, 44-48.
(62) Qi, G.; Wang, Q.; Xu, J.; Trébosc, J.; Lafon, O.; Wang, C.; Amoureux, J.-P.; Deng, F. *Angewandte Chemie International Edition* **2016**, *55*, 15826-15830.
(63) Venkatesh, A.; Hanrahan, M. P.; Rossini, A. J. *Solid State Nucl. Magn. Reson.* **2017**, *84*, 171-181.
(64) Duong, N. T.; Rossi, F.; Makrinich, M.; Goldbourt, A.; Chierotti, M. R.; Gobetto, R.; Nishiyama, Y. *J. Magn. Reson.* **2019**, *308*, 106559.
(65) Carnahan, S. L.; Lampkin, B. J.; Naik, P.; Hanrahan, M. P.; Slowing, I. I.; VanVeller, B.; Wu, G.; Rossini, A. J. *J. Am. Chem. Soc.* **2019**, *141*, 441-450.
(66) Venkatesh, A.; Luan, X.; Perras, F. A.; Hung, I.; Huang, W.; Rossini, A. J. *Phys. Chem. Chem. Phys.* **2020**, *22*, 20815-20828.
(67) Nagarkar, S. S.; Kurasho, H.; Duong, N. T.; Nishiyama, Y.; Kitagawa, S.; Horike, S. *Chemical Communications* **2019**, *55*, 5455-5458.
(68) Chen, L.; Lu, X.; Wang, Q.; Lafon, O.; Trébosc, J.; Deng, F.; Amoureux, J.-P. *J. Magn. Reson.* **2010**, *206*, 269-273.
(69) Nimerovsky, E.; Gupta, R.; Yehl, J.; Li, M.; Polenova, T.; Goldbourt, A. *J. Magn. Reson.* **2014**, *244*, 107-113.
(70) Lu, X.; Lafon, O.; Trebosc, J.; Tricot, G.; Delevoye, L.; Mear, F.; Montagne, L.; Amoureux, J. P. *J. Chem. Phys.* **2012**, *137*, 144201.
(71) Grey, C. P.; Veeman, W. S.; Vega, A. J. *J. Chem. Phys.* **1993**, *98*, 7711-7724.
(72) van Eck, E. R. H.; Janssen, R.; Maas, W. E. J. R.; Veeman, W. S. *Chem. Phys. Lett.* **1990**, *174*, 428-432.
(73) Jarvis, J. A.; Haies, I. M.; Williamson, P. T. F.; Carravetta, M. *Phys. Chem. Chem. Phys.* **2013**, *15*, 7613-7620.
(74) Hung, I.; Gor'kov, P.; Gan, Z. *J. Chem. Phys.* **2019**, *151*, 154202.

(75) Celinski, V. R.; Weber, J.; Schmedt auf der Günne, J. *Solid State Nucl. Magn. Reson.* **2013**, *49-50*, 12-22.
(76) Van Meervelt, L.; De Wael, K.; Zeegers-Huyskens, T. *J. Mol. Struct.* **1995**, *356*, 183-190.
(77) Goetz, J. M.; Schaefer, J. *J. Magn. Reson.* **1997**, *127*, 147-154.
(78) Perras, F. A.; Johnson, R. L.; Wang, L. L.; Schwartz, T. J.; Kobayashi, T.; Dumesic, J. A.; Shanks, B. H.; Johnson, D. D.; Pruski, M. *J. Am. Chem. Soc.* **2017**, *139*, 2702–2709.
(79) Merwin, L. H.; Sebald, A. *Solid State Nucl. Magn. Reson.* **1992**, *1*, 45-47.
(80) Bryce, D. L.; Sward, G. D.; Adiga, S. *J. Am. Chem. Soc.* **2006**, *128*, 2121-2134.
(81) Hamaed, H.; Pawlowski, J. M.; Cooper, B. F. T.; Fu, R.; Eichhorn, S. H.; Schurko, R. W. *J. Am. Chem. Soc.* **2008**, *130*, 11056-11065.
(82) Pandey, M. K.; Kato, H.; Ishii, Y.; Nishiyama, Y. *Phys. Chem. Chem. Phys.* **2016**, *18*, 6209-6216.
(83) Hung, I.; Gan, Z. *J. Phys. Chem. Lett.* **2020**, *11*, 4734-4740.
(84) Iuga, D.; Corlett, E. K.; Brown, S. P. *Magn. Reson. Chem.* **2021**, *59*, 1089-1100.
(85) Fuess, H.; Hohlwein, D.; Mason, S. A. *Acta Crystallogr. B* **1977**, *33*, 654-659.
(86) Chan, J. C. C.; Eckert, H. *J. Magn. Reson.* **2000**, *147*, 170-178.
(87) Bertmer, M.; Eckert, H. *Solid State Nucl. Magn. Reson.* **1999**, *15*, 139-152.
(88) Bertmer, M.; Züchner, L.; Chan, J. C. C.; Eckert, H. *The Journal of Physical Chemistry B* **2000**, *104*, 6541-6553.
(89) Bak, M.; Rasmussen, J. T.; Nielsen, N. C. *J. Magn. Reson.* **2000**, *147*, 296-330.
(90) Tosner, Z.; Vosegaard, T.; Kehlet, C.; Khaneja, N.; Glaser, S. J.; Nielsen, N. C. *J. Magn. Reson.* **2009**, *197*, 120-134.
(91) Tosner, Z.; Andersen, R.; Stevenss, B.; Eden, M.; Nielsen, N. C.; Vosegaard, T. *J. Magn. Reson.* **2014**, *246*, 79-93.
(92) Clark Stewart, J.; Segall Matthew, D.; Pickard Chris, J.; Hasnip Phil, J.; Probert Matt, I. J.; Refson, K.; Payne Mike, C. *Z. Kristallogr. Cryst. Mater.* **2005**, *220*, 567.
(93) Perdew, J. P.; Burke, K.; Ernzerhof, M. *Phys. Rev. Lett.* **1996**, *77*, 3865-3868.
(94) Tkatchenko, A.; Scheffler, M. *Phys. Rev. Lett.* **2009**, *102*, 073005.
(95) Vanderbilt, D. *Phys. Rev. B* **1990**, *41*, 7892-7895.
(96) Yates, J. R.; Pickard, C. J.; Mauri, F. *Phys. Rev. B* **2007**, *76*, 024401.
(97) Pickard, C. J.; Mauri, F. *Phys. Rev. B* **2001**, *63*, 245101.